IEEE Photonics Journal
An IEEE Photonics Society Publication

Open Access

Frequency-Doubling of Femtosecond Pulses in "Thick" Nonlinear Crystals With Different Temporal and Spatial Walk-Off Parameters

Volume 8, Number 6, December 2016

N. Apurv Chaitanya
A. Aadhi
S. Chaitanya Kumar
M. V. Jabir
G. K. Samanta
M. Ebrahim-Zadeh

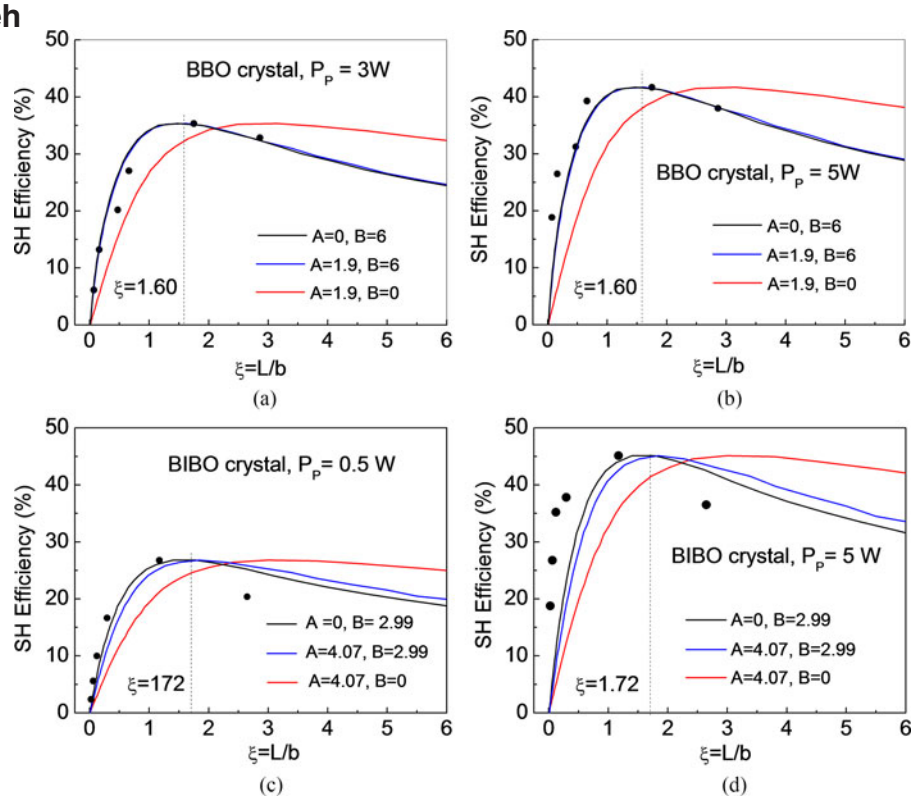

DOI: 10.1109/JPHOT.2016.2626198
1943-0655 © 2016 IEEE

Frequency-Doubling of Femtosecond Pulses in "Thick" Nonlinear Crystals With Different Temporal and Spatial Walk-Off Parameters

N. Apurv Chaitanya,[1] A. Aadhi,[1] S. Chaitanya Kumar,[2] M. V. Jabir,[1] G. K. Samanta,[1] and M. Ebrahim-Zadeh[2,3]

[1]Photonic Sciences Laboratory, Physical Research Laboratory, Navarangpura, Ahmedabad 380 009, Gujarat, India
[2]ICFO-Institut de Ciencies Fotoniques, Castelldefels 08860, Barcelona, Spain
[3]Institucio Catalana de Recerca i Estudis Avancats (ICREA), Barcelona 08010, Spain

DOI:10.1109/JPHOT.2016.2626198

Manuscript received September 10, 2016; revised November 2, 2016; accepted November 4, 2016. Date of publication November 8, 2016; date of current version December 8, 2016. This work was supported in part by the Ministry of Economy and Competitiveness, Spain, through Project nuOPO (TEC2015-68234-R), in part by the European Commission (project Mid-TECH, H2020-MSCA-ITN-2014), in part by the Generalitat de Catalunya (AGAUR, project SGR 2014-2016), in part by the Severo Ochoa Excellence Grant SEV-2015-0522, and in part by the Fundació Privada Cellex. Corresponding author: G. K. Samanta (e-mail: gsamanta@prl.res.in).

Abstract: We present a comparative study on frequency-doubling characteristics of femtosecond laser pulses in thick nonlinear crystals with different temporal and spatial walk-off parameters. Using single-pass second harmonic generation (SHG) of 260 fs pulses at 1064 nm from a high-average-power femtosecond Yb-fiber laser in 5-mm-long crystals of β-BaB_2O_4 (BBO) and BiB_3O_6 (BIBO), we find that for comparable values of temporal and spatial walk-off parameters in each crystal, the optimum focusing condition for SHG is more strongly influenced by spatial walk-off than temporal walk-off. It is also observed that under such conditions, the Boyd and Kleinman theory commonly used to define the optimum focusing condition for frequency-doubling of cw and long-pulse lasers is also valid for SHG of ultrafast lasers. We also investigate the effect of focusing on the spectral, temporal, and spatial characteristics of the second harmonic (SH) radiation, as well as angular acceptance bandwidth for the SHG process, under different temporal and spatial walk-off conditions in the two crystals.

Index Terms: Harmonic generation and mixing, nonlinear optics, materials, ultrafast lasers, fiber lasers, upconversion, visible lasers.

1. Introduction

The development of ultrafast femtosecond laser sources in different spectral regions is of great interest for a variety of applications, including spectroscopy [1], [2], material processing [3], [4], and pumping of optical parametric oscillators [5], [6]. The restricted fluorescence bandwidth of solid-state and fiber gain media confines the wavelength coverage of mode-locked ultrafast lasers to limited regions in the near and mid-infrared. Nonlinear frequency conversion techniques provide a highly effective approach to circumvent this limitation, providing access to new wavelength regions unavailable to conventional ultrafast lasers [7]. Among different nonlinear processes, second

harmonic generation (SHG) is typically used to reach the shorter wavelengths, including the visible [8], [9] and ultraviolet regions [10]. In particular, single-pass SHG offers the simplest configuration, which can be realized in a most compact and cost-effective system design [11], [12]. On the other hand, because of the single-pass nature of this technique, the nonlinear gain is generally low, but this can be improved by using crystals with high optical nonlinearity, noncritical phase-matching (NCPM), long interaction length, as well as by increasing the intensity of the input fundamental. By exploiting quasi-phase-matched nonlinear crystals such as PPKTP and MgO:sPPLT with long interaction length under NCPM in single-crystal [13] and cascaded multi-crystal schemes [14], the single-pass SHG technique has been shown to be highly effective in achieving overall conversion efficiencies of $>$50% into the green in the continuous-wave (cw) regime. On the other hand, in the picosecond time-scale, the use of long birefringent crystals such as BiB_3O_6 (BIBO) [9] and LiB_3O_5 (LBO) [15] has enabled high-power single-pass SHG into the green. In the ultrafast femtosecond regime, however, the use of increasingly long crystals does not necessarily lead to higher gain in the SHG process, as other crystal parameters including temporal walk-off can play an increasingly significant role in the overall conversion efficiency, even in the presence of NCPM. In the absence of NCPM, as is commonly the case in birefringent crystals, spatial walk-off becomes an important additional factor that limits SH efficiency. In this case, increasing the crystal length also does not necessarily lead to higher conversion efficiency, given the trade-off between the crystal length and the focusing parameter of the fundamental, which is dependent on spatial walk-off [16]. Therefore, the attainment of the highest conversion efficiency in SHG, as well as other nonlinear frequency conversion processes, in the ultrafast femtosecond time-scales, requires careful optimization of focusing to account for both spatial and temporal walk-off. For a given nonlinear crystal of a certain physical length and under a specific phase-matching geometry and a given input fundamental laser of certain pulse duration and intensity, the optimization of focusing is the most critical factor in the attainment of the highest conversion efficiency and output power.

Here, we present a comparative study on the optimum focusing condition for SHG of femtosecond pulses in two different nonlinear crystals with different temporal and spatial walk-off parameters. The optimum focusing conditions for efficient SH conversion of cw or long-pulse lasers have been theoretically predicted in the seminal work of Boyd and Kleinman (BK) [16] and subsequently verified experimentally [13]. However, the optimum focusing condition in the presence of temporal walk-off arising from the use of ultrafast lasers can be different from that of the cw and long-pulse lasers. Previously, efforts have been made to model and determine the optimum focusing condition for SHG of ultrafast lasers [17]–[20]. However, these efforts require experimental verification. Here we present a systematic experimental study on the optimum focusing condition for single-pass SHG of ultrashort femtosecond pulses in two nonlinear crystals having different spatial and temporal walk-off parameters and their comparison with the existing theoretical models [17]–[19]. For our study, we deploy an ultrafast Yb-fiber laser at 1060 nm as the input fundamental, together with birefringent nonlinear crystals of β-BaB_2O_4 (BBO) and BIBO under critical phase-matching, for SHG into the green. It is found that for each crystal with comparable values of A and B parameters defining temporal and spatial walk-off, respectively, the optimum focusing condition for SHG is more strongly influenced by spatial walk-off than temporal walk-off. It is also observed that for comparable values of temporal and spatial walk-off parameters A and B, respectively, BK theory is also valid for SHG of femtosecond pulses.

2. Experimental Configuration

The schematic of the experimental set up is shown in Fig. 1 and is similar to that in our earlier report [21]. The pump source is an ultrafast Yb-fiber laser (Fianium, FP1060-5-fs) delivering 5 W of average power in pulses of 260 fs duration at 78 MHz repetition rate. When operated at maximum power, the laser provides a linearly polarized output beam in TEM_{00} spatial profile with $M^2 < 1.3$. The laser wavelength is centered at 1060 nm. The spectrum is flat with small modulation and has a full-width at half-maximum (FWHM) bandwidth of 15 nm. The time-bandwidth product of the pump pulse is $\sim$1.04, which is substantially larger than the value of 0.315 for a transform-limited

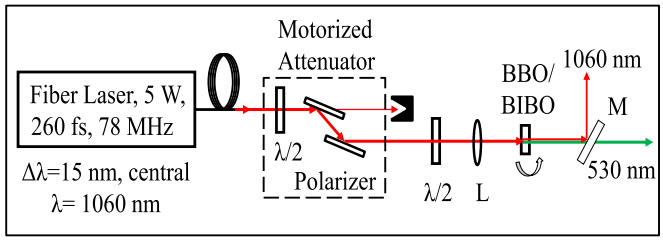

Fig. 1. Experimental design of the single-pass SHG of the femtosecond Yb-fiber laser. $\lambda/2$: half-wave plate; BBO and BIBO: nonlinear crystals, L: lens; M: mirror.

sech^2 pulse. For SHG experiments, we use two crystals, BBO and BIBO, to study the performance of the frequency-doubling process with regard to all important output parameters as a function of focusing under different spatial and temporal walk-off conditions. Both crystals are 5-mm-long and $4 \times 8\,\text{mm}^2$ in aperture. In each case, the input power to the crystal is controlled using a motorized attenuator, consisting of two polarizers and a half-wave plate (HWP). Another HWP is used to obtain the desired polarization for optimum phase-matching in the crystal. A set of six lenses of focal length, $f = 25$, 50, 100, 150, 200, and 300 mm, are used for focusing the fundamental beam into the nonlinear crystal in each case, and a separation mirror, M, filters out the fundamental from the SH output. The BBO crystal is cut at an internal angle $\theta = 22.9°$ for type I (ee $\rightarrow$ o) SHG at a fundamental wavelength of 1064 nm at normal incidence. The BIBO crystal is cut at $\theta = 168.5°$ ($\varphi = 90°$) in the optical *yz*-plane for type I (ee $\rightarrow$ o) phase-matching at normal incidence. Both crystals are antireflection (AR)-coated on both faces at 1064 and 532 nm. For these phase-matching geometries, the spatial walk-off angle in BIBO and BBO are $\rho = 26.1$ mrad and $\rho = 55.85$ mrad, respectively. The corresponding values of group velocity mismatch (GVM) are $\beta = 173\,\text{fs/mm}$ in BIBO and $\beta = 84.8\,\text{fs/mm}$ in BBO. The spatial walk-off length (L_S) and temporal walk-off length (L_T) are defined as $L_S = 2w_p/tan(\rho)$ and $L_T = \tau_p/\beta$, respectively, where w_p is the pump beam waist radius inside the crystal, and τ_p is the pump pulse width. For a pump pulse width, $\tau_p = 260\,\text{fs}$, the temporal walk-off length is thus calculated to be $L_T = 1.5\,\text{mm}$ in BIBO and $L_T = 2.95\,\text{mm}$ in BBO.

On the other hand, measuring the pump beam waist radius in the BBO and BIBO crystals for lenses of different focal lengths, $f = 25$-300 mm, we can estimate the spatial walk-off length, L_S, to vary over 0.48-5.25 mm in BBO, and 1.02-11.39 mm in BIBO. While BBO has twice larger spatial walk-off angle than BIBO under the same focusing condition, the GVM for BBO is almost half that of BIBO. Such differences in spatial and temporal walk-off in the two crystals enable us to study the dependence of optimum focusing for SHG on the two parameters. The relevant characteristics of the BIBO and BBO crystals used in the present study are listed in Table 1.

3. Results and discussions

3.1. Optimum focusing condition

To study the effects of temporal and spatial walk-off parameters on focusing dependence of SHG efficiency, we pumped both BBO and BIBO crystals at maximum available fundamental power and measured the SH efficiency under different focusing conditions. We define the focusing parameter, $\xi = L/b$ [16], where L is the crystal length, b is the confocal parameter of the pump beam given by $b = 2n\pi {w_p}^2/\lambda_p$, n is the refractive index of the crystal, w_p the beam waist radius, and λ_p is the fundamental wavelength. To vary ξ, we focused the pump beam to different waist radii using various focusing lenses. By measuring the beam waist diameter of the pump beam using a scanning beam profiler for six lenses, $f = 25$, 50, 100, 150, 200, and 300 mm, we calculated ξ for both crystals under different focusing conditions. The results, together with the corresponding spatial walk-off lengths, L_s, are listed in Table 2.

TABLE 1
PARAMETERS OF BIBO AND BBO CRYSTALS

Crystals / Parameters	BIBO	BBO
Crystal length	L=5 mm	L=5 mm
Phase-matching type	Type-I ($ee \rightarrow o$)	Type-I ($ee \rightarrow o$)
Phase-matching angle	θ=168.5°(ϕ=90°)	θ=22.9°
Effective nonlinear coefficient	d_{eff}=2.96 pm/V	d_{eff}=2.01 pm/V
Spatial walk-off	ρ=26.1 mrad	ρ=55.85 mrad
Spatial walk-off length	L_S=0.48-5.25 mm	L_S=1.02-11.39 mm
Temporal walk-off	β=173 fs/mm	β=84.8 fs/mm
Temporal walk-off length	L_T=1.5 mm	L_T=2.95 mm

TABLE 2
FOCUSING PARAMETERS IN BIBO AND BBO CRYSTALS

	BIBO			BBO		
Lens, f (mm)	w_p (μm)	ξ	L_s (mm)	w_p (μm)	ξ	L_s (mm)
25	13.37	2.63	1.02	14.91	2.86	0.48
50	20.12	1.16	1.54	17.11	1.75	0.61
100	40.21	0.29	3.08	27.88	0.47	1.18
150	62.95	0.12	4.82	33.07	0.16	1.99
200	89.16	0.06	6.83	55.81	0.07	3.05
300	148.75	0.02	11.39	85.37	0.02	5.25

Figure 2 shows the variation of the SH efficiency in BBO and BIBO crystals as a function of the focusing parameter, ξ. For completeness of the study, we present here the relevant results obtained in our earlier work on the BIBO crystal [21] in Fig. 4(b). The filled circles correspond to the experimental efficiency values obtained under the six different focusing conditions. The solid curves are calculations for different conditions of temporal walk-off (A) and spatial walk-off (B) based on different theoretical models described below. As evident from Fig. 2(a), the SH conversion efficiency obtained with the BBO crystal increases with tighter focusing, reaching a maximum values of 41.65% at $\xi = 1.75$, and decreases with further increase in ξ. Similarly, as shown in Fig. 2(b), for the BIBO crystal the maximum SH efficiency of 46.5% is reached for $\xi = 1.16$, beyond which, there is once again a decline. Under similar experimental conditions, BIBO provides higher SH efficiency than BBO, mainly due to its superior nonlinear coefficient.

To calculate the optimal value of ξ for the highest SH efficiency under our experimental conditions, we used three theoretical models, which are represented by the different color curves in Fig. 2. The theoretical models correspond to three different cases involving temporal walk-off (A) and spatial walk-off (B):

Case 1: Blue curve represents the theoretical model that includes the effects of both temporal and spatial walk-off ($A \neq 0$, $B \neq 0$) in optimum focusing [17].

Case 2: Black curve represents the theoretical model that considers only spatial walk-off ($A = 0$, $B \neq 0$) [16].

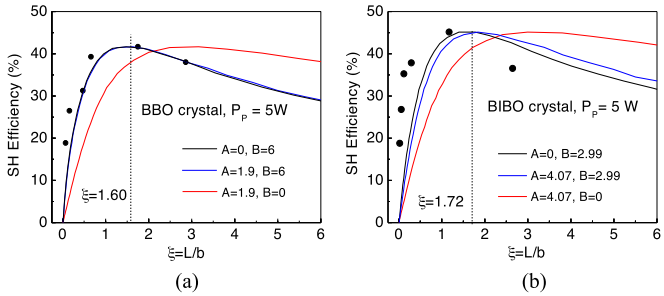

Fig. 2. Variation of SH efficiency as a function of focusing parameter, ξ, for (a) BBO and (b) BIBO at the maximum input fundamental power of 5 W. The solid curves are theoretical calculations for three different cases involving spatial and temporal walk-off. Blue curve: includes both spatial and temporal walk-off. Black curve: includes only spatial walk-off. Red curve: includes only temporal walk-off. Dotted lines at $\xi = 1.60$ and $\xi = 1.72$ represent theoretical optimum focusing for BBO and BIBO crystals.

Case 3: Red curve represents the model that considers only temporal walk-off ($A \neq 0$, $B = 0$) [19].

The parameters representing the effect of temporal walk-off (A) and spatial walk-off (B) are given by [17]

$$A = \sqrt{\frac{(\alpha^2 + 16)\ln 2}{8}}\,\frac{\beta L}{\tau_p} \tag{1}$$

$$B = \frac{\rho\sqrt{k_1 L}}{2} \tag{2}$$

and

$$\sigma = \sqrt{A^2 + 4B^2\xi} \tag{3}$$

Here, α represents the amount of chirp in the fundamental pulse, β is the group velocity mismatch between the fundamental and SH pulse [17], ρ is the spatial walk-off angle in the crystal, τ_p is the fundamental pulse width, k_1 is the wave-vector of the fundamental radiation, and L is the crystal length. Substituting the parameter values for BBO ($\beta = 84.75$ fs/mm, $\rho = 55.85$ mrad) and BIBO ($\beta = 173$ fs/mm, $\rho = 26.1$ mrad) crystals, and the pulse duration (FWHM) of the fundamental, $\tau_p = 260$ fs, into (2) and (3), we calculate the temporal and spatial walk-off parameters for the 5-mm-long BBO and BIBO crystals to be $A = 1.9$, $B = 6$ and $A = 4.07$, $B = 2.9$, respectively. For simplicity, we consider that our fiber laser has negligible chirp ($\alpha = 0$).

In order to calculate the dependence of SH efficiency on ξ for the three different cases, we use the dimensionless function $h_m(A, B, \xi)$ [16]

$$h_m(A, B, \xi) = \frac{1}{4\xi}\int_{-\xi}^{\xi}\int_{-\xi}^{\xi}\frac{e^{-\sigma^2(\tau_{x1}-\tau_{x2})^2/4\xi^2}\,d\tau_{x1}\,d\tau_{x2}}{(1 - i\tau_{x1})(1 - i\tau_{x2})} \tag{4}$$

where $\tau_{x1} = 2z/b_{x1}$ and $\tau_{x2} = 2z/b_{x2}$, with b_{x1} and b_{x2} being the confocal parameters of the Gaussian fundamental beam in the horizontal and vertical directions, respectively, and σ as defined by (3). Using the values of A and B, we can then derive the SH efficiency as a function of ξ under the three conditions. For $A \neq 0$ and $B \neq 0$, we derive the blue curves in Fig. 2, which account for the effect of both temporal and spatial walk-off in optimum focusing (case 1), as in [17]. For no temporal walk-off ($A = 0$), the same function is represented by the black curves, which include only the effect of spatial walk-off (case 2), as in [16]. With no spatial walk-off ($B = 0$), the calculation results in the red curves, which include only the effect of temporal walk-off (case 3), as in [19].

As evident from Fig. 2(a) and Fig. 2(b), there is a relatively strong discrepancy between the red curve and our experimental data for each crystal, whereas the blue and black curves are in good

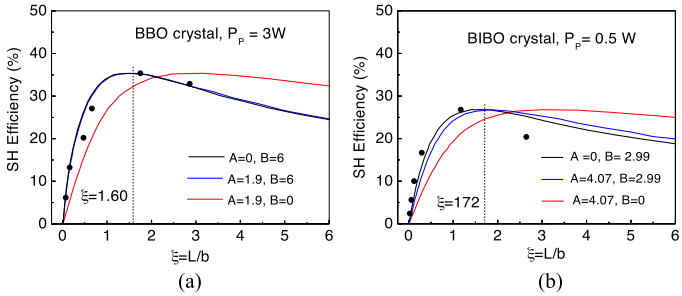

Fig. 3. Variation of SH efficiency as a function of focusing parameter, ξ, for (a) BBO and (b) BIBO at lower fundamental average powers of 3 W and 0.5 W, respectively.

agreement with both sets of measurements. This confirms that the finite spatial walk-off plays a vital role in the variation of conversion efficiency with the focusing strength in both crystals, as expected. On the other hand, the nearly identical behavior of the blue and black curves in Fig. 2(a) suggests that the temporal walk-off has negligible or no effect on optimum focusing condition in the BBO crystal, which is due to its small temporal walk-off parameter ($A = 1.9$) arising from a lower GVM ($\beta = 84.75$ fs/mm). Our experimental findings also agree with the earlier theoretical predictions in [17] and [18]. In case of BIBO, shown in Fig. 2(b), we again find close correlation between the blue and the black curves. This implies that although the BIBO crystal has a larger temporal walk-off parameter ($A = 4.07$), almost twice that of BBO ($A = 1.9$), its role in the optimization of SH conversion efficiency with focusing still remains small. The experimental data in Fig. 2(b) are most closely in agreement with the black curve predicted by BK theory [16]. This suggests that even if temporal walk-off is more significant in BIBO, spatial walk-off still remains the dominant factor dictating the optimum focusing condition. On the other hand, for large values of GVM in the nonlinear crystal and/or shorter fundamental pulses, temporal walk-off can play an increasingly significant role in the optimization of focusing for SHG [17], [19]. By fitting our experimental data to BK theory [16], represented by the black curves in Fig. 2(a) and 2(b), we find the optimum values of $\xi = 1.72$ for BBO and $\xi = 1.6$ for BIBO. The shift in the optimum ξ value towards tighter focusing in BIBO as compared to BBO is due to the higher spatial walk-off parameter in BBO ($B = 6$) relative to BIBO ($B = 2.99$), which is consistent with BK theory [16].

It is also to be noted from Fig. 2(a) that although the blue and black curves closely fit the experimental data for BBO, one can clearly observe a more significant deviation between the blue and black curves in the case of BIBO in Fig. 2(b). This deviation can be attributed to the saturation effect and back-conversion at higher fundamental powers arising from the higher nonlinear gain in BIBO. To verify this, we measured the conversion efficiency in both crystals as a function of focusing at lower fundamental powers of 3 W in BBO and 0.5 W in BIBO, with the results shown in Fig. 3. As evident from Fig. 3(a), for BBO the experimental data is again in good agreement with the theoretical calculation (blue and black lines), as in Fig. 2(a). At the same time, as can be seen in Fig. 3(b), the experimental data for the BIBO crystal at lower fundamental powers are now also in very close agreement with the theoretical calculation unlike in Fig. 2(b), in the absence of saturation and back-conversion. It is to be noted that BK theory [16] is valid under the approximation of low fundamental depletion and, hence, small conversion efficiency.

From the above study, we thus find that in the presence of both double-refraction and GVM, the optimum focusing condition for SHG of femtosecond pulses in both BBO and BIBO is much more strongly influenced by spatial walk-off than temporal walk-off. Although the behavior might be different for very high values of GVM [19], we can conclude that for moderate temporal and spatial walk-off, the BK theory [16] relevant to frequency-doubling of cw and long-pulse lasers, is also valid for SHG of ultrafast lasers.

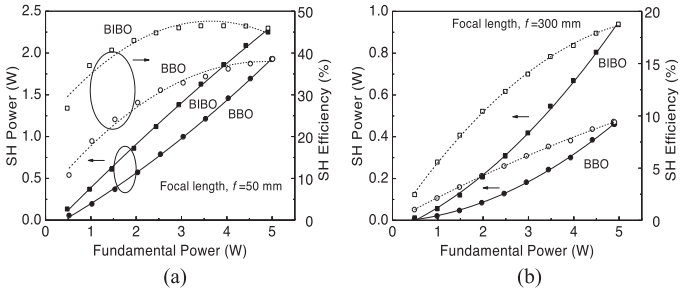

Fig. 4. SH power and efficiency scaling results for BBO and BIBO crystals at different focusing conditions of (a) $\xi = 1.75$ (BBO), $\xi = 1.16$ (BIBO), and (b) $\xi = 0.02$ for both the crystals.

3.2. Power scaling and saturation effects

To study saturation effects at high conversion efficiency, we investigated the power scaling properties of BBO and BIBO crystals under two different focusing conditions. First, we focused the pump beam using a lens of focal length, $f = 50$ mm, to achieve optimum focusing condition of $\xi = 1.75$ in BBO and $\xi = 1.16$ in BIBO, for maximum SH efficiency, and measured the output power as a function of the input fundamental power. The results are shown in Fig. 4. As evident from Fig. 4(a), under optimum focusing conditions, the SH power from the BIBO crystal increases almost linearly with input power, resulting in an output power of 2.25 W for 5 W of fundamental power. While one should expect a quadratic dependence of SH power on the pump power, the linear behavior of the SH power with pump power can be attributed to the saturation effect. This is also evident from the SH efficiency which remains almost constant at ~46.5% for fundamental powers above ~2.5 W. On the other hand, for the BBO crystal, we observe slight quadratic dependence of the SH power on pump power, resulting in a single-pass output power of 2.07 W for 5 W of input power. However, in this case, the SH efficiency exhibits small or no saturation effect. The maximum SH efficiency in the BBO crystal is measured to be ~41.65% at 5 W of fundamental power. To gain more insight into the saturation effects in the two crystals, we repeated the same set of measurements, but this time by loosely focusing the pump beam using a lens of focal length, $f = 300$ mm, providing the same focusing factor of $\xi = 0.02$ in both the crystals. The results are shown in Fig. 4(b). As evident from the plots, both crystals now show clear quadratic variation of SH power with input pump power, resulting in 0.46 W (0.95 W) of green power at 9.4% (18.6%) conversion efficiency in BBO (BIBO). The conversion efficiency is almost linear with respect to pump power for both crystals, indicating the absence of saturation effect under loose focusing.

To understand the saturation effect in both crystals under similar experimental conditions, we consider the SHG conversion efficiency in the plane-wave approximation, with no depletion of the fundamental wave, as given by [22]

$$\eta = \frac{P_{2\omega}(L)}{P_{\omega}(0)} = \eta_{norm}\left[\frac{P_{\omega}L^2}{A}\right] sinc^2\left(\frac{\Delta kL}{2}\right)$$

$$\eta_{norm} = \frac{8\pi^2 d_{\text{eff}}^2}{n_{\omega}^2 n_{2\omega} c\varepsilon_0 \lambda_{\omega}^2} \tag{5}$$

where η_{norm} is the normalized SHG conversion efficiency; P_{ω} is the input fundamental power; A is the fundamental beam area; d_{eff} is the effective nonlinear coefficient; n_{ω} and $n_{2\omega}$ are refractive indices of the crystal at fundamental and SH wavelengths, respectively; ε_0 is the permittivity of free space; c is the velocity of light; λ_{ω} is the fundamental wavelength; Δk is the phase mismatch; and L is the crystal length. Under perfect phase-matching ($\Delta k = 0$) and similar experimental conditions (same pump power and beam area), the normalized SH efficiency of BIBO (η_{norm}^{BIBO}) is ~2.2 times that of BBO (η_{norm}^{BBO}). This is due to the higher nonlinear coefficient of BIBO ($d_{\text{eff}} = 2.96$ pm/V) compared to BBO ($d_{\text{eff}} = 2.01$ pm/V). Now, we can take the ratio of the SH efficiency of BIBO and BBO crystals shown in Fig. 4(a) and 4(b), and plot the ratios as a function of the input fundamental

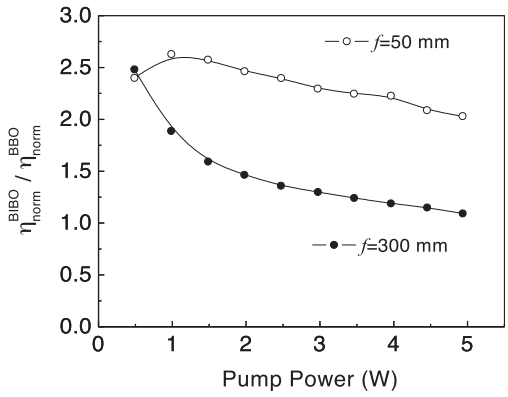

Fig. 5. Variation in the ratio of SH efficiencies of BIBO and BBO crystals as a function of input pump power focused using two lenses of focal length, $f = 50$ mm and $f = 300$ mm.

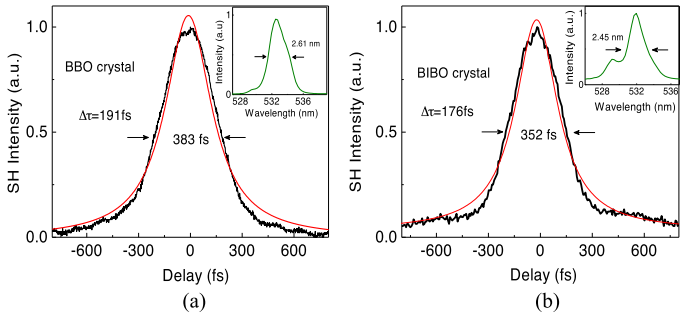

Fig. 6. Typical intensity autocorrelation traces of the green pulses generated from (a) BBO and (b) BIBO at the maximum output power. (Inset) Corresponding SH spectra centered at 532 nm.

power. The result is shown in Fig. 5, where we see that for optimum focusing in both crystals (using $f = 50$ mm lens), a value of $\eta_{norm}^{BIBO}/\eta_{norm}^{BBO} \sim$2.4-2 is maintained at lower powers up to $\sim$1 W, but drops to 1.09 at the higher pump powers up to 5 W. On the other hand, under loose focusing (using $f = 300$ mm lens), the ratio of the SH efficiency remains almost constant at $\eta_{norm}^{BIBO}/\eta_{norm}^{BBO} \sim$2.6-2.02 for all fundamental powers. This observation clearly indicates that for higher values of focusing parameter, ξ, corresponding to tighter focusing, the SH efficiency in BIBO is increasingly saturated. The result also accounts for the slight deviation of the experimental data in Fig. 2(b) from the black curve based on the BK theory [16].

3.3. Temporal and spectral characterization of SH pulses

We also characterized the output pulse duration and spectral bandwidth of the green radiation generated by the BBO and BIBO crystals, with the results shown in Fig. 6. The measurements were performed under optimum focusing condition for both crystals (using a $f = 50$ mm lens), while generating maximum green power when pumping at $\sim$5 W of fundamental power. The intensity autocorrelation traces of the SH pulses generated by the two crystals are shown in Fig. 6(a) and (b). As can be seen, the autocorrelation profiles conform to Lorentzian pulse shape with measured FWHM duration of $\sim$383 fs in BBO and $\sim$352 fs in BIBO. Taking account of the deconvolution factor (0.5) for Lorentzian pulse shape, we estimate a SH pulse width of 191 fs for BBO and 176 fs for BIBO. We also measured the spectrum of the generated green radiation for both crystals using a CCD-based spectrometer. The results are shown in the insets of Fig 6(a) and Fig. 6(b). The measurements result in a FWHM spectral bandwidth of 2.35 nm for BBO and

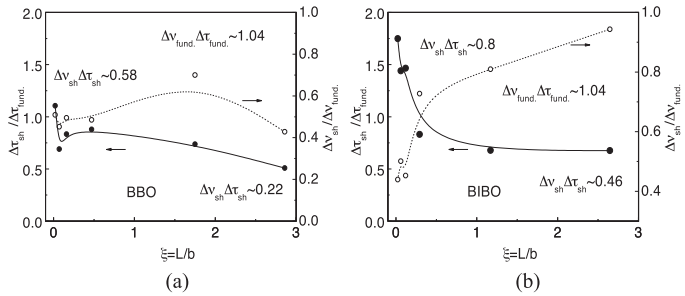

Fig. 7. Variation of the ratio of SH pulse duration and FWHM spectral bandwidth with respect to that of the input fundamental as a function of the focusing parameter, ξ, in (a) BBO and (b) BIBO. Loose focusing is the condition when the confocal parameter, *b*, is much larger than the crystal length, *L*. In other words, the loose focusing corresponds to the condition, $\xi \ll 1$.

2.45 nm in BIBO, both centered at 532 nm. The time-bandwidth product ($\Delta\tau\Delta\upsilon$) of the green radiation generated by the two crystals is thus calculated to be ~0.54 for BBO and ~0.46 for BIBO, both close to the transform limit. The deviation of the SH pulses from the transform limit is mainly attributed to the non-transform-limited fundamental pulses ($\Delta\tau\Delta\upsilon = 1.04$). Pulse broadening of the fundamental due to the group velocity dispersion (GVD) is calculated to be only a few femtosecond, and thus has negligible effect on the SHG process and output temporal duration. We also analyzed the pump spectrum before and after the crystal. We saw no distortion in the pump spectrum after the crystal. The flat spectrum of the fiber pump laser shows substantial depletion verifying high single-pass SHG efficiency, as noted earlier.

3.4. Effect of focusing on temporal and spectral characteristics

We also studied the variation in pulse duration and spectral bandwidth of the generated green radiation as a function of the focusing parameter, ξ, for both crystals. We pumped the crystals at the maximum available fundamental power of ~5 W and measured the pulse duration and spectral bandwidth of the SH output pluses in each case. We then plotted the ratio of the SH pulse duration and spectral bandwidth to that of the input fundamental as a function of ξ. The results are shown in Fig. 7, where the pulse duration and spectral bandwidth of the pump are ~260 fs and ~15 nm, respectively. For completeness of the current study, we have reproduced the results of Fig. 7(b) from [21]. As evident from Fig. 7(a), the ratio of the SH pulse duration (solid circles) to the pump pulse duration in the BBO crystal has a small variation from 1.1 to 0.51 as the focusing parameter increases from $\xi = 0.02$ to 2.86. The corresponding ratio of the SH spectral bandwidth (open circles) relative to that of the pump varies from 0.51 to 0.42 with increasing ξ, reaching a maximum of 0.7 at $\xi = 1.75$. On the contrary, the BIBO crystal shows significant variation in the SH pulse duration and spectral bandwidth with focusing. As can be seen from Fig. 7(b), the ratio of the SH pulse duration to that of the pump (solid circles) decrease rapidly from 1.75 to 0.83 for an increase in the focusing parameter from $\xi = 0.02$ to 0.29, beyond which the ratio remains almost constant up to $\xi = 2.86$. At the same time, the ratio of the SH spectral bandwidth to that of the pump (open circles) shows inverse behavior to the temporal pulse duration. With the increase in ξ, the spectral bandwidth ratio shows a sharp increase from 0.44, but in the tighter focusing regime ($\xi > 0.29$) it shows a slower variation with focusing. The time-bandwidth product of the generated SH pulses is calculated to vary over $\Delta\tau_{sh}\Delta\upsilon_{sh} \sim 0.58 - 0.22$ for BBO and $\Delta\tau_{sh}\Delta\upsilon_{sh} \sim 0.8 - 0.46$ for the BIBO crystal with the increase in the focusing parameter from $\xi = 0.02$ to 2.86 and, hence, with tighter focusing.

The dependence of temporal pulse duration and spectral bandwidth on focusing for different values of temporal and spatial walk-off in the two crystals can be explained as follows. The confocal parameter, *b*, determines the effective length of the nonlinear crystal over which efficient nonlinear interaction takes place. For a fixed physical length of the crystal (*L*), the value of *b* reduces

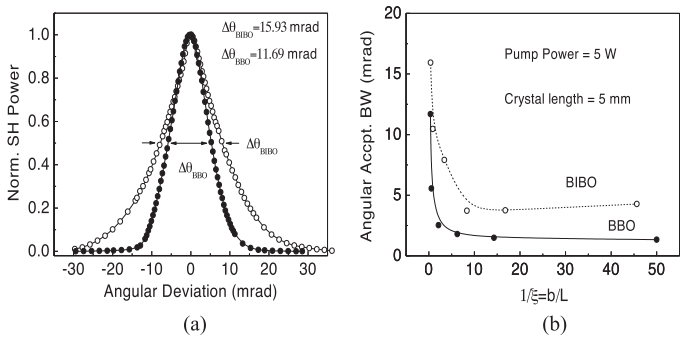

Fig. 8 (a) Variation of the normalized SH power as a function of the internal angular deviation measure at the maximum SH power for both BBO and BIBO. (b) Variation of the SH angular acceptance bandwidth as function of the focusing parameter for both BBO and BIBO crystals.

with tighter focusing. However, in the presence of spatial walk-off, the effective interaction length of the crystal is further reduced. As a result, an increase in the spectral acceptance bandwidth of the crystal is expected. Therefore, for a given spectral bandwidth of the fundamental ($\Delta\nu_{\text{fund}}$) that is larger than the spectral acceptance bandwidth of the physical crystal, more pump bandwidth can be exploited in the SHG process with tighter focusing and stronger spatial walk-off, hence increasing the bandwidth of the SH radiation. As evident from the open circles in both Fig. 7(a) and Fig. 7(b), we also observe this experimentally. The bandwidth of the generated SH radiation is large under tight focusing and decreases with loose focusing, becoming almost constant for $\xi < 1$ and $\xi < 0.4$ for BBO and BIBO crystals, respectively. Another important factor influencing the temporal duration and spectral bandwidth of the SH pulses is the temporal walk-off length of the crystal. Under our experimental conditions, the BBO and BIBO crystals have temporal walk-off length of $L_T = 2.95$ mm and 1.5 mm, resulting in a ratio of physical length to temporal walk-off length (L/L_T) of 1.69 and 3.3, respectively. As theoretically predicted earlier [19], we experimentally observe that in the case of BBO, which has a low L/L_T as compared to BIBO, there is a small variation in the SH pulse duration with focusing and, hence, with the effective interaction length over which temporal walk-off between the fundamental and SH pulses occurs.

3.5. Effect of focusing on angular acceptance bandwidth

We also investigated the effect focusing on angular phase-matching acceptance bandwidth for frequency doubling of femtosecond pulses under different temporal and spatial walk-off conditions in the two crystals, with the results shown in Fig. 8. We used a lens of $f = 25$ mm to focus the fundamental beam into the two crystals, resulting in a focusing parameter of $\xi = 2.86$ in BBO and $\xi = 2.63$ in BIBO. We then measured the angular acceptance bandwidth of 5-mm-long BBO and BIBO crystals. The result is shown in Fig. 8(a), where it is evident that BIBO exhibits a wider angular acceptance bandwidth ($\Delta\theta_{\text{BIBO}} = 15.93$ mrad) than BBO ($\Delta\theta_{\text{BBO}} = 11.69$ mrad). These experimentally measured values are significantly larger than the theoretical angular acceptance bandwidth for 5-mm BIBO ($\Delta\theta_{\text{BIBO}} = 4.62$ mrad) and 5-mm BBO ($\Delta\theta_{\text{BBO}} = 2.30$ mrad) [23]. Such deviation is expected and is attributed to tight focusing ($\xi > 2$), as well as the wide spectral bandwidth ($\Delta\lambda \sim 15$ nm) of the fundamental beam. However, with increasingly loose focusing, the angular acceptance bandwidths are expected to approach the theoretical values. This is confirmed in Fig. 8(b), where the variation of experimentally measured angular acceptance bandwidths of the BBO and BIBO crystal, obtained using lenses of decreasing focal length, is plotted as a function of the focusing parameter. Such variation of angular acceptance bandwidth with focusing factor can be understood as follows. As we know, the effective length of the nonlinear crystal changes with focusing. Under very tight focusing, the effective interaction length is significantly reduced compared to the physical length of the crystal, resulting in broadening of the acceptance bandwidth and its devi-

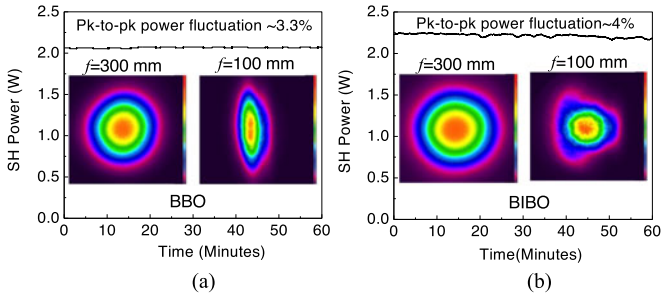

Fig. 9. Long-term power stability over 1 hour and spatial beam profile of the SH beam generated from (a) BBO and (b) BIBO nonlinear crystals, while operated at respective optimum focusing conditions. The SH spatial profiles are recoded for lenses of focal length, $f = 300$ and 100 mm, for both the crystals.

ation from the value under perfect phase matching. Under loose focusing, the effective interaction length of the crystal is increased, restricting the angular acceptance for phase-matching toward the perfect phase-matching condition. However, when the effective interaction length becomes equal to the physical length, further loosening of focusing has no further impact, resulting in a constant angular acceptance bandwidth. This is evident in Fig. 8(b), where the angular acceptance bandwidth of both BBO and BIBO crystals is very large under tight focusing (low value of $1/\xi$), gradually decreasing with looser focusing, and finally under very loose focusing (high value of $1/\xi$), becoming almost constant and close to the theoretical value. The angular acceptance bandwidth in case of 5-mm-long BBO crystal varies from 11.69 mrad to 1.33 mrad with increasingly looser focusing from $1/\xi = 0.35$ to 50. Similarly, for BIBO, we observe angular acceptance bandwidth variation from 15.9 mrad to $\sim$4.28 mrad for looser focusing from $1/\xi = 0.38$ to 8.3. However, it is to be noted that at any given focusing the angular acceptance bandwidth of BIBO crystal is wider than that of BBO crystal, which is expected due to the lower spatial walk-off in BIBO.

3.6. Power stability and spatial beam profile

We further investigated the output power stability and spatial quality of the generated SH output beam in both crystals under optimum focusing condition for maximum SH power and efficiency, using a lens of focal length, $f = 50$ mm, and at the full pump power of $\sim$5 W. The results are shown in Fig. 9. As can be seen, both BBO and BIBO crystals exhibit very similar SH power stability with a peak-to-peak fluctuation as low as $\sim$3.3% for BBO and $\sim$4% for BIBO. Such observation indicates that temporal and spatial walk-off parameters do not play any role in the instability in SH output power, as expected. However, spatial walk-off parameter is expected to make a definite contribution to the spatial profile of the SH output beam. To verify the effect of spatial walk-off, we loosely focused ($\xi \sim 0.02$) the pump beam using a lens of focal length, $f = 300$ mm, at maximum pump power, and measured the far-field energy distribution of the SH beam at a distance $>$2 m from the crystal in each case using a CCD-based beam profiler. The results are shown in the inset of Fig. 9(a) for BBO and Fig. 9(b) for BIBO. As evident, the SH beam from both crystals has excellent TEM_{00} spatial profile with circularity, of $>$90% for BBO and $>$98% for BIBO. The higher beam circularity in BIBO under same focusing condition is clearly due to the lower spatial walk-off in BIBO ($B = 2.99$) compared to BBO ($B = 6$). However, with the increase in the focusing factor, ξ, under tighter focusing, the circularity of the SH output beam was observed to degrade but more severely and rapidly in the case of BBO than BIBO. When using a focusing lens of focal length, $f = 100$ mm, the circularity of the SH output beam was reduced to $>$34% for BBO ($\xi = 0.47$) and $>$74% for BIBO ($\xi = 0.29$). The results are shown in the inset of Fig. 9(a) for BBO and Fig. 9(b) for BIBO. For the strongest focusing, using a lens of focal length, $f = 25$ mm, resulting in the highest value of $\xi = 2.86$ in BBO and $\xi = 2.63$ for BIBO, the SH beam circularity was reduced to as low as a few percent in both cases due to the onset of high spatial walk-off. We measured the M^2-value of the SH beam

generated by the BIBO crystal under optimum focusing condition ($\xi = 1.16$) to be $M_X^2 \sim 4.02$ and $M_Y^2 \sim 1.78$, clearly confirming the deterioration of SH beam from a perfect TEM_{00} distribution. In the case of BBO, however, under optimum focusing condition ($\xi = 1.75$), we could not measure its M^2-value due to high ellipticity of the SH beam. From these measurements, we can conclude that while the higher SH conversion efficiency and output power can be realized under tighter focusing conditions, this will result in a reduction in beam circularity and a deviation from TEM_{00} profile. The circularity of the SH output beams can, however, be readily improved using cylindrical beam shaping optics.

4. Conclusions

In conclusion, we have experimentally studied frequency-doubling of high-average-power femtosecond pulses from an ultrafast Yb-fiber laser at 1064 nm into the green using thick nonlinear crystals with different temporal and spatial walk-off parameters. Using single-pass SHG in BBO and BIBO, we have investigated the effect of focusing on the SH efficiency and found the optimum focusing conditions for the 5-mm-long BBO and BIBO, respectively, in the presence of spatial and temporal walk-off. These results are in good agreement with the theoretical calculations performed using practical values. Under optimum focusing conditions, we were able to generate up to 2.25 and 2.05 W of green output in single-pass configuration for a maximum available fundamental power of ~5 W at 78 MHz pulse repetition rate. We also investigated the effect of focusing on the SH power and efficiency saturation. Spectral and temporal characterization of the generated SH pulses have been performed, and the variation of output spectral bandwidth and pulse duration as function of the focusing parameter, ξ, has been studied. Moreover, the angular acceptance bandwidths of both crystals for SHG into the green have been measured under various focusing conditions and their dependence on the effective interaction length resulting from the spatial and temporal walk-off has been analyzed. This comparative study provides a systematic analysis for the attainment of optimum SH performance with regard to output power, spectrum, pulse duration, and beam quality of the generated green beam in the presence of limiting factors of spatial and temporal walk-off in thick BBO and BIBO crystals for single-pass SHG of the state-of-the-art femtosecond Yb-fiber lasers. An important overall conclusion of the present study is that the performance of the SHG process is far more strongly dictated by spatial walk-off than temporal walk-off.

References

[1] N. Dudovich, D. Oron, and Y. Silberberg, "Single-pulse coherently controlled nonlinear Raman spectroscopy and microscopy," *Nature*, vol. 418, pp. 512–514, 2002.

[2] T. Ideguchi, A. Poisson, G. Guelachvili, T. W. Hänsch, and N. Picqué, "Adaptive dual-comb spectroscopy in the green region," *Opt. Lett.*, vol. 37, pp. 4847–4849, 2012.

[3] J. Chang, B. Warner, E. Dragon, and M. Martinez, "Precision micromachining with pulsed green lasers," *J. Laser Appl.*, vol. 10, no. 6, pp. 285–291, 1998.

[4] K. Sugioka and Y. Cheng, "Ultrafast lasers—reliable tools for advanced materials processing," *Light: Sci. Appl.*, vol. 3, no. 4, p. e149, 2014.

[5] S. Chaitanya Kumar and M. Ebrahim-Zadeh, "Fiber-laser-based green-pumped picosecond MgO:sPPPLT optical parametric oscillator," *Opt. Lett.*, vol. 38, pp. 5349–5352, 2013.

[6] G. K. Samanta, S. Chaitanya Kumar, A. Aadhi, and M. Ebrahim-Zadeh, "Yb-fiber-laser-pumped, high-repetition-rate picosecond optical parametric oscillator tunable in the ultraviolet," *Opt. Exp.*, vol. 22, pp. 11476–11487, 2014.

[7] M. Ebrahim-Zadeh, "Mid-infrared ultrafast and continuous-wave optical parametric oscillators," in *Solid-State Mid-Infrared Laser Sources* (Topics in Applied Physics 89), I. T. Sorokina and K. L. Vodopyanov, Eds. Berlin, Germany: Springer-Verlag, 2003, pp. 179–218.

[8] M. Ebrahim-Zadeh and S. Chaitanya Kumar, "Yb-fiber-laser-pumped ultrafast frequency conversion sources from the mid-infrared to the ultraviolet," *IEEE J. Sel. Topics Quantum Electron.*, vol. 20, 2014, Art. no. 7600519.

[9] S. Chaitanya Kumar and M. Ebrahim-Zadeh, "High-power, fiber-pumped, picosecond green source based on bismuth triborate," *Laser Phys.*, vol. 24, p. 025401, 2014.

[10] G. K. Samanta, S. Chaitanya Kumar, A. Aadhi, and M. Ebrahim-Zadeh, "Yb-fiber-laser-pumped, high-repetition-rate picosecond optical parametric oscillator tunable in the ultraviolet," *Opt. Exp.*, vol. 22, pp. 11476–11487, 2014.

[11] G. K. Samanta *et al.*, "High-power, continuous-wave, second-harmonic generation at 532 nm in periodically poled KTiOPO4," *Opt. Lett.*, vol. 33, pp. 2955–2957, 2008.

[12] M. Ebrahim-Zadeh, "Efficient ultrafast frequency conversion sources for the visible and ultraviolet based on BiB3O6," *IEEE J. Sel. Topics Quantum Electron.*, vol. 13, no. 3, pp. 679–691, May/Jun. 2007.
[13] G. K. Samanta, S. Chaitanya Kumar, and M. Ebrahim-Zadeh, "Stable, 9.6 W, continuous-wave, single-frequency, fiber-based green source at 532 nm," *Opt. Lett.*, vol. 34, pp. 1561–1563, 2009.
[14] G. K. Samanta, S. Chaitanya Kumar, K. Devi, and M. Ebrahim-Zadeh, "Multicrystal, continuous-wave, single- pass second-harmonic generation with 56% efficiency," *Opt. Lett.*, vol. 35, pp. 3513–3515, 2010.
[15] S. Chaitanya Kumar, J. Canals Casals, J. Wei, and M. Ebrahim-Zadeh, "High-power, high-repetition-rate performance characteristics of β-BaB2O4 for single-pass picosecond ultraviolet generation at 266 nm," *Opt. Exp.*, vol. 23, pp. 28091–28103, 2015.
[16] G. D. Boyd and D. A. Kleinman, "Parametric interactions of focused Gaussian light beams," *J. Appl. Phys.*, vol. 39, pp. 3897–3641, 1968.
[17] H. Wang and A. M. Weiner, "Efficiency of short-pulse type-I second-harmonic generation with simultaneous spatial walk-off, temporal walk-off, and pump depletion," *IEEE J. Quantum Electron.*, vol. 39, no. 12, pp. 1600–1618, Dec. 2003.
[18] A. M. Weiner, A. M. Kan'an, and D. E. Leaird, "High-efficiency blue generation by frequency doubling of femtosecond pulses in a thick nonlinear crystal," *Opt. Lett.*, vol. 23, no. 18, pp. 1441–1443, 1998.
[19] S. M. Saltiel, K. Koynov, B. Agate, and W. Sibbett, "Second-harmonic generation with focused beams under conditions of large group-velocity mismatch," *J. Opt. Soc. Amer. B*, vol. 21, pp. 591–598, 2004.
[20] S. Erkin, A. Knoesen, and A Dienes, "Ultrashort-pulse second-harmonic generation. I. Transform-limited fundamental pulses," *J. Opt. Soc. Amer., B*, vol. 12, pp. 1704–1712, 1995.
[21] N. Apurv Chaitanya, A. Aadhi, R. P. Singh, and G. K. Samanta, "Type-I frequency-doubling characteristics of high-power, ultrafast fiber laser in thick BIBO crystal," *Opt. Lett.*, vol. 39, pp. 5419–5422, 2014.
[22] S. Chaitanya Kumar, G. K. Samanta, K. Devi, and M. Ebrahim-Zadeh, "High-efficiency, multicrystal, single-pass, continuous-wave second harmonic generation," *Opt. Exp.*, vol. 19, pp. 11152–11169, 2011.
[23] SNLO software developed by Sandia National Laboratories. [Online]. Available: www.sandia.gov/imrl/XWEB1128/sstal.htm